Introduction to wind turbine design

Gijs van Kuik, Wim. Bierbooms
DUWIND, Delft University Wind Energy Research Institute

1. Introduction

This chapter deals with some basic principles of wind energy conversion. Focus is on wind modeling, the aerodynamic process, concept choices for power control and safety, optimization of annual energy yield, and some characteristics of blade dynamics.
For a detailed treatment of the material, Ref. 1 is a recommended textbook.

2. Wind modeling

2.1 Structure of the atmospheric boundary layer

Wind is moving air caused by pressure differences in the atmosphere, initiated by temperature differences. At large heights (~1000 m) the wind is not perpendicular to the isobars but parallel to it due to the Coriolis force (perpendicular to the wind direction, caused by the rotation of the earth). This wind is denoted the geostrophic wind.

G	:	pressure gradient force	Ug	:	geostrophic wind
C	:	Coriolis force	U	:	wind at the ground
W	:	drag force (friction)			

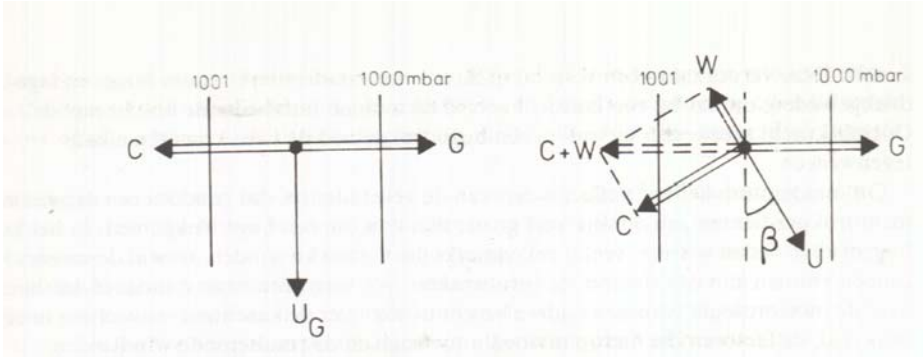

Fig. 1: Isobars and direction of velocity in case of balance of all forces

At lower heights friction will lead to wind shear: a reduction of the wind magnitude (especially in the so-called surface layer, 0 to 60 or 100 m above ground level) and a change in the wind direction (especially above the surface layer: the Ekman layer).

There are two causes of the friction:

a) Thermic. The friction depends on the stability of the atmosphere: stable (above a cold surface), neutral or unstable (above a hot surface; the warm air will rise and lead to mixing of air layers with different velocities)
b) Mechanic. The friction is a function of the terrain roughness, characterised by the roughness length z_0.

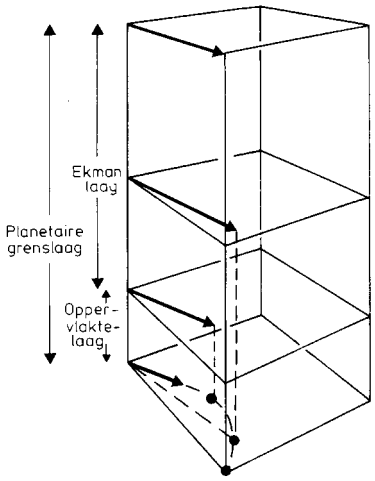

Fig. 2: The Ekman layer

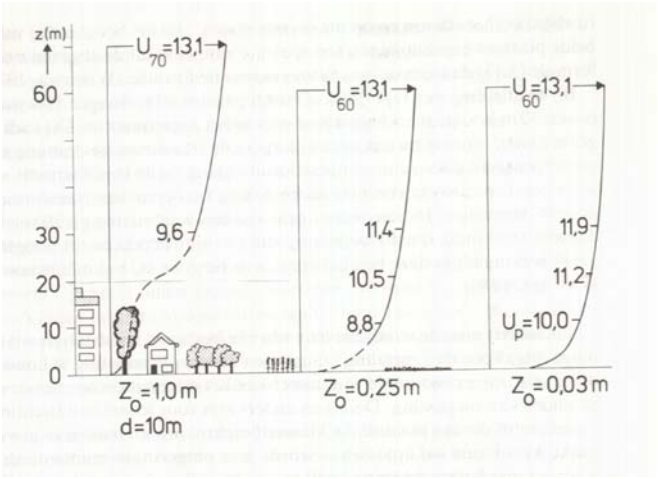

Fig. 3: The wind shear due to roughness z_0

For not too low wind speeds (above 5 m/s) the atmosphere may be treated as neutral, and the following equation is valid for the (mean) wind speed at some height with respect to the wind speed at a reference height (e.g. a measured wind speed):

$$V(h) = V(h_{ref})\left(\frac{\ln(h/z_0)}{\ln(h_{ref}/z_0)}\right) \qquad [1]$$

This expression can be used to calculate the wind speed at hub height from wind speed observations or models where the wind speed is given at a standard height of 10 m. The most simple relationship to describe the wind profile (i.e. the horizontal wind speed U as function of height h) is a power law:

$$\frac{U(h_1)}{U(h_2)} = \left(\frac{h_1}{h_2}\right)^{\alpha} \qquad [2]$$

This is a non-physical expression, used in some standards, which gives reasonable results for the correct value of α (usually in the order of 0.1 for onshore applications).

2.2 Estimation of the mean wind speed at a given location

It is not possible to determine a map of the mean wind speeds due to the large local variations of the roughness length. To overcome this problem a so-called potential wind speed has been defined: this is the wind speed at a standard height of 10 m which would exist in case the local roughness length would be equal to the standard value of 0.03 m. The KNMI has processed such a map for the Netherlands based on several years of wind measurements (ref. 2). Similar maps exist for other countries (ref.3). The mean wind speed at a given location with known roughness length z_o follows from fig. 4 combined with equation {1} or [2].

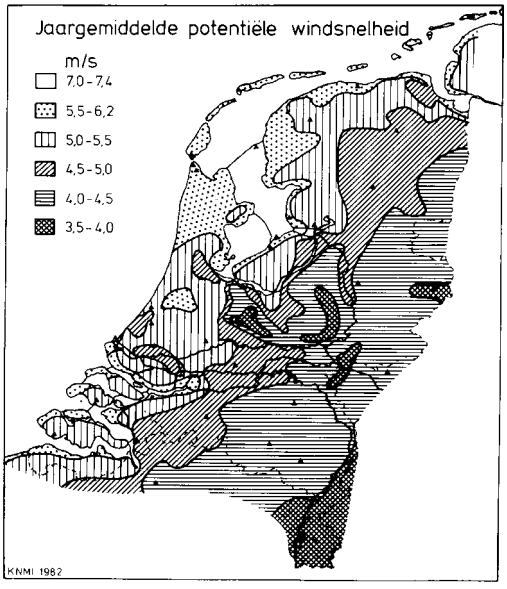

Fig. 4: potential windspeed in the Netherlands

2.3 Wind statistics

Wind is extremely variable: it fluctuates continuously in speed and direction. This variability extends over an enormous range of time scales. This variability results from the many different physical phenomena which influence the wind; each has its own characteristic effects and occurs over a characteristic range of time (and length) scales. The figure shows a (fictional, similar to Van der Hoven) power spectrum of wind speed variations (showing the contribution of different time scales to the total variability).

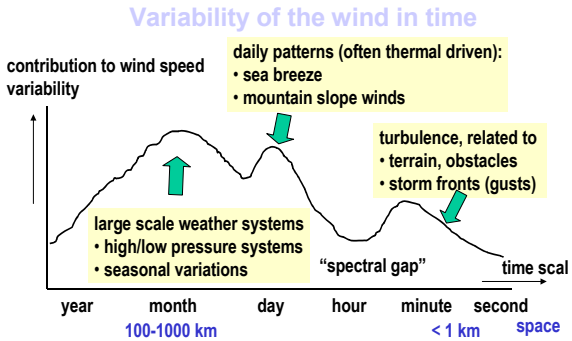

Fig. 5: time scale of wind speed variations

On the scale "second to minutes" : stationary turbulence, caused by friction of the wind with the surface, by wakes of obstacles, by thermal instability (warm air rises); non stationary "turbulence" related to cold fronts, hail storms etc. On the scale of " hours to days": passing of the above mentioned non stationary phenomena; thermally driven daily circulations as sea breezes, mountain slope winds. On the scale of "days to weeks": changes due to development and passing of large scale weather systems. On the scale of weeks to months": seasonal differences, related to regional and global temperature differences; On the scale of "years to years": year to year differences caused by cyclic solar activity, "El Nino" type of phenomena, long term trends eg. global warming !).

The picture shows that time scales between "many minutes"and "a few hours" contribute much less to the overall variability than smaller and especially larger time scales. This means that if one compares an one hour average with the next one hour average, these values are likely to be more similar than comparing two successive week averages or second averages. The low variability around these middle time scales is called the spectral gap. The very existence of the spectral gap makes it possible to split the analysis of wind into two main parts A and B, where A is the variability due to "turbulence" and where B is the variability due to "climatology". It has turned out to be convenient to separate these two parts by using a 10 minute average (or up to 1 hour, this choice is not very critical).

The frequency distribution of the mean wind speed exhibits an important characteristic: it can be assumed to be distributed according to the cumulative Weibull distribution function which is determined by two parameters only:

$$F(U) = 1 - e^{-(U/a)^k} \qquad [3]$$

Here F is the probability of a wind speed smaller than U, a is the Weibull scale factor and k is the Weibull form or shape factor.

Another, maybe more familiar form is the following:

$$f(U) = \frac{k}{U}\left(\frac{U}{a}\right)^k e^{-(U/a)^k} \qquad [4]$$

Here f is the continuous probability density function of wind speed U, see figure 6. The Weibull parameters a and k can be calculated by a fit matching the observed data (measured or hindcast). This can be done for each of the twelve wind direction sectors

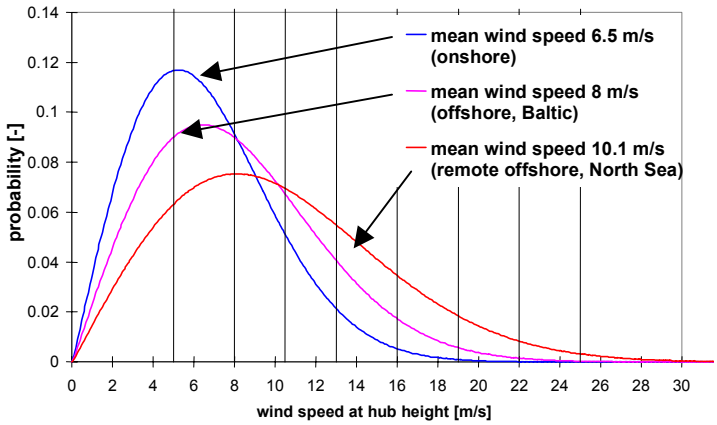

Fig.6: Examples of Weibull distributions

(of 30 degrees each), see figure 7. The parameter a is proportional to the mean wind speed with a given k.

By straightforward combination of the Weibull distribution and the power curve of the wind turbine (power as function of the wind speed at hub height; both averaged over 10-min) the annual energy yield can be determined, see chapter 4.

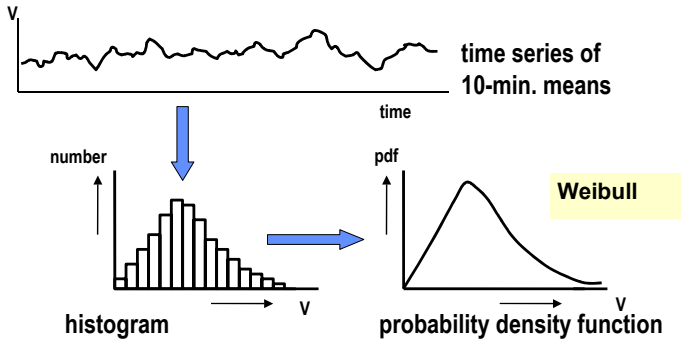

Fig. 7: from time series to pdf.

2.4 Turbulence

Variation of the wind speed within a period of 10-min is called turbulence (the part of fig. 5 at the right of the spectral gap).
These fluctuations have a Gaussian (normal: 'bell-shaped') distribution. The ratio between the standard deviation and the 10-min. mean wind speed is called turbulence intensity. Turbulence does not effect the energy yield but it is vital for the dynamic wind turbine loading.
The characteristic time scales of turbulence varies between a second to minutes; the corresponding length scales range from a meter to hundreds of meters. The spatial variation of turbulence is 'felt' by a rotating wind turbine blade as temporal ones; this phenomenon is denoted rotational sampling, see figure 9. The frequency of the turbulence as seen by a stationary observer (indicated in fig. 9 by the

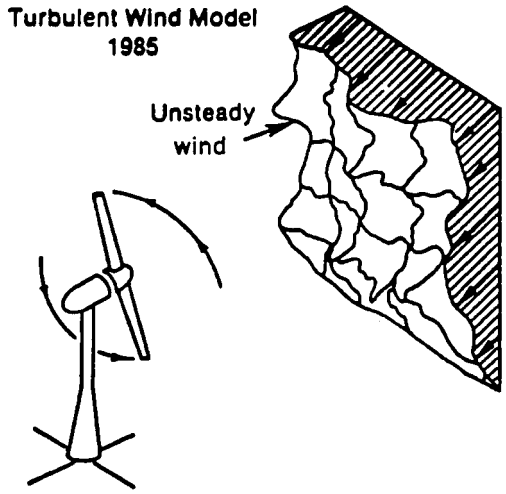

Fig. 8: Visualisation of turbulence

Rotational sampling of turbulence

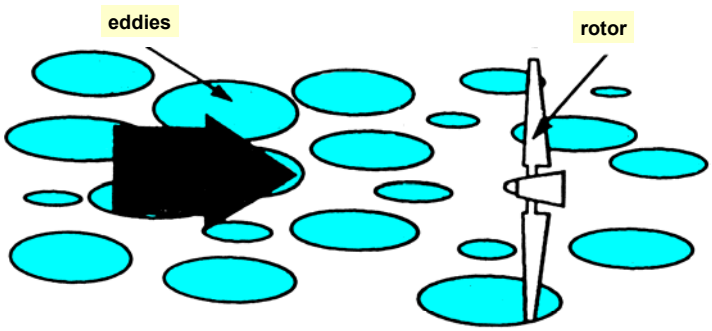

Fig. 9: rotational sampling

size of the turbulence area) will increase when seen by a co-rotating observer. The blades slice the turbulent spots with a frequency determined by the rotational speed and the number of blades. It results in a dynamic wind loading with main frequencies equal to the rotor frequency (so-called '1P') and its multiples (2P, 3P, …nP). Apart from turbulence the following wind loads result in periodic wind loads which may lead to fatigue: wind shear, yawed flow and tower shadow. Note: also gravity acts as a periodic load (in the so-called lead-lag direction: parallel to the rotor plane).

Nowadays, it is common practice to generate 3D stochastic wind fields, for several mean wind speeds, to account for turbulence in the simulation of wind turbines. For such a simulation, the parameters describing the turbulence spectrum should be known as well as the turbulence intensity.
The number of occurrences of each mean wind speed during the design lifetime of the wind turbine follows from the Weibull distribution.

2.5 Extreme wind speeds

The KNMI has also compiled a map of extreme wind speeds (10-min. or 1 hour mean values). Usually a return period of 50 years is applied; i.e. the extreme wind speeds occur *on average* once in 50 years.
For the determination of the extreme wind loads, the turbulence on top of the extreme wind speeds must be taken into account. For this purpose, standards specify deterministic wind gust shapes. Ongoing research aims at a more precise, stochastic description of gusts.

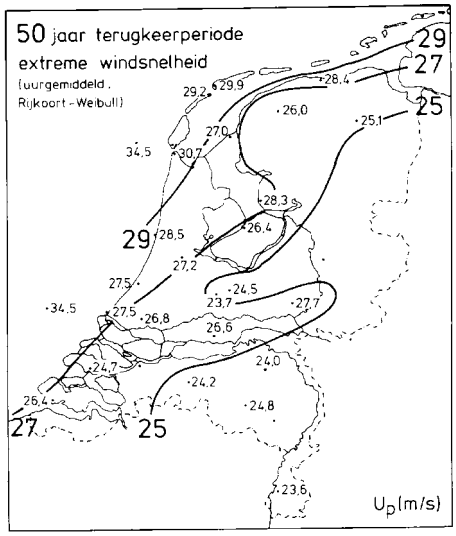

Fig. 10: map of extreme wind speeds

3. Principles of aerodynamic theory

All current design codes for wind turbine rotors are based on the Blade Element Momentum theory (BEM). This theory is of an elegant simplicity, with modest calculation requirements, and reasonably successful in predicting performance and loads. However, it is not able to predict all flow conditions with sufficient accuracy. Due to its simplicity, BEM is easily extended by engineering rules to cover these deficiencies. Engineering rules are still being developed, since old problems are still unsolved, and new aerodynamic problems occur with the increasing size of wind turbines. Both BEM as well as some engineering rules are discussed.

One way of classifying the types of flow encountered in rotor-aerodynamics is based on the spatial and time scales involved. Other classifications are possible, but this one is of use in understanding the 'engineering' solutions to the problems. Two families of scales can be distinguished:

- spatial scale: the rotor diameter D; time scale D/U_w, a few seconds (global flow field); This is the domain of the momentum balances incorporated in BEM.
- spatial scale: the blade chord c; time scale: $c/\Omega r$ a few hundreds of a second (blade flow field). This is the domain of the blade element aerodynamics.

The flow fields are linked in the sense that the global flow field is determined by the rotor forces (determined by the blade flow field). In turn, this blade flow field, or the blade inflow velocity is determined by the global induction (velocity change due to the global pressure field). In the global flow field the rotor is modeled as an internal pressure-jump boundary condition. In the blade flow field real aerofoil data are used to calculate the aerodynamic forces.

3.1 Blade Element Momentum theory

BEM theory consists of a mix of conservation laws. Figure 11 shows a control volume in the flow with length $U\Delta t$, and cross-section A. With ρ the density, the mass in the control volume is $\rho U\Delta tA$, so the mass flow passing through A per second is:

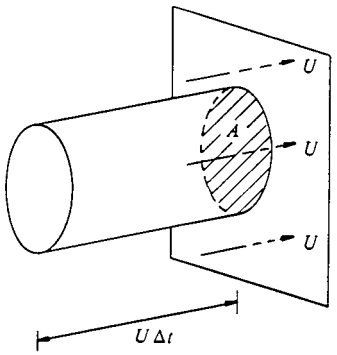

Fig.11: definition of mass flow

$$\text{mass flow} \qquad m = \rho UA \qquad [5a]$$

similarly, the momentum and energy per second are:

$$\text{momentum flow} \qquad mU = \rho U^2 A \qquad [5b]$$

$$\text{energy flow} \qquad \tfrac{1}{2}mU^2 = \tfrac{1}{2}\rho U^3 A \qquad [5c]$$

The momentum and energy are affected by the action of the rotor force D, acted upon the flow. The simplest representation of the rotor is the actuator disc, see figure 12.

The rotor force (thrust) D is represented by a uniform pressure jump Δp, where

$$\Delta p = D / A \qquad [6]$$

With the control volume given in figure 12, the momentum and energy balances read:

$$D = \rho A V_1 (U - V_e) \quad [7]$$

$$P = \rho A V_1 \left(\tfrac{1}{2} U^2 - \tfrac{1}{2} V_e^2\right) \quad [8]$$

in which P is the power, the work done per second. The force D acting on a flow with velocity V produces:

$$P = D V_1 \quad [9]$$

Combining [7,8,9] yields the well-known result that the velocity at the disc is the average of the velocities up- and downstream.

$$V_1 = \tfrac{1}{2}(U + V_e) \quad [10]$$

Now the induction factor is introduced, to make the velocities non-dimensionless:

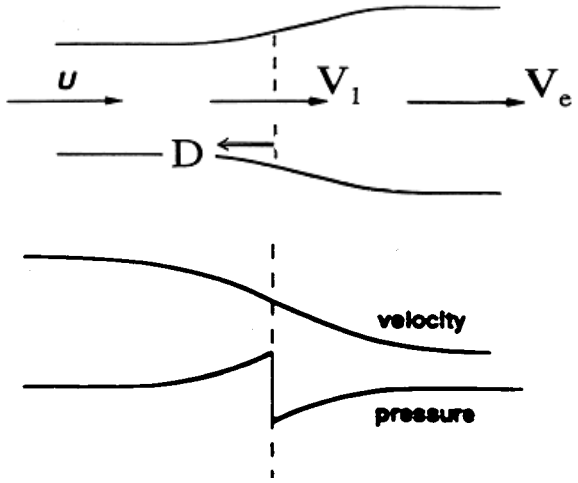

Fig. 12: actuator disc flow

$$a = \frac{(U - V_1)}{U} \quad [11]$$

so a expresses the relative change of the velocity at the disc. Substitution in the previous equations provides:

$$D = \tfrac{1}{2} \rho U^2 A \; 4a(1 - a) \quad [12]$$

$$P = \tfrac{1}{2} \rho U^3 A \; 4a(1 - a)^2 \quad [13]$$

The thrust or drag D and power D are made dimensionless by division by ½ρU²A and ½ρU³A respectively, leading to the thrust- en power coefficients:

$$C_{d_{ax}} = \frac{D}{\tfrac{1}{2} \rho U^2 A} = 4a(1 - a) \quad [14]$$

$$C_p = \frac{P}{\tfrac{1}{2} \rho U^3 A} = 4a(1 - a)^2 \quad [15]$$

Differentiating to the induction factor a yields the maximum efficiency:

$$C_{p_{\max}} = \frac{16}{27} \approx 0.59 \quad for \quad a = \frac{1}{3} \quad [16]$$

This result is named after Betz (Ref. 4), although it is known (afterwards) that Lanchester was the first to formulate this (Ref. 5). The maximum thrust coefficient is

1.0, for a = ½.. Physically, the occurrence of a maximum is easy to explain: a very large rotor force decelerates the flow too much, by which the mass flow through the rotor disc is small. A small rotor force affects the mass flow only little, but does not extract energy from the flow.

Glauert (Ref. 6) made this actuator disc theory applicable for real calculations, by applying it to flow annuli, instead of the entire flow tube. Figure 13 shows such an annulus. The parts of the rotor blades inside the annulus are called the blade-elements. Glauert imposed the assumption that the flow and forces in each annulus is independent of the other annuli. Although this assumption is proved to be wrong, it works very well. The mutual interaction between the annuli is only noticeable near the tip and blade roots, where large gradients of the blade loading occur.

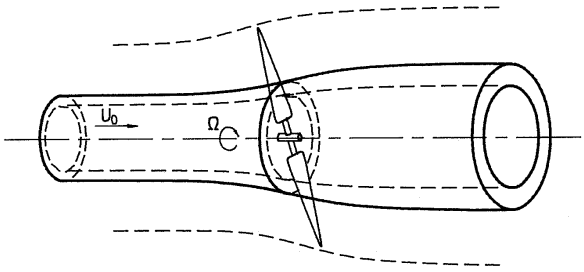

Figure 13: The annulus as control volume for Blade Element Momentum analysis

More assumptions are involved: in each annulus the velocity is uniform, and the force exerted by the blade elements is thought to be distributed uniform with respect to the azimuth. Given these assumptions, all actuator disc results can be applied within the annuli.

The final step in the BEM theory is to formulate how the blade-element force D is generated. Figure 14 shows a cross-section through a blade at radius r, seen from a co-rotating observer at the blade tip, looking towards the rotor center. The blade moves to the left, the wind comes from below. The aerofoil experiences a resultant velocity V_{res}, resulting from the vector addition of the rotational speed Ωr and the local wind speed U(1-a).

The difference α between the chordline of the aerofoil and the velocity vector determines the aerodynamic force R for a given aerofoil. This force is conveniently decomposed in a lift vector, perpendicular to V_{res} and the drag vector, parallel to V_{res}. The angle of attack α can be controlled by changing the rotor speed Ω and adjusting the pitch angle of the blade θ. It changes, uncontrolled, by variations in the wind speed U. Ω, θ and U are independent parameters, whereas a, the induction parameter, is the dependent parameter that links the global momentum analyses to the blade element analysis. The lift and drag on the element are a function of this induction a, which in turn is a function of the total axial force in the annulus. The contribution to the torque of the rotor is Lsinφ-Dcosφ.

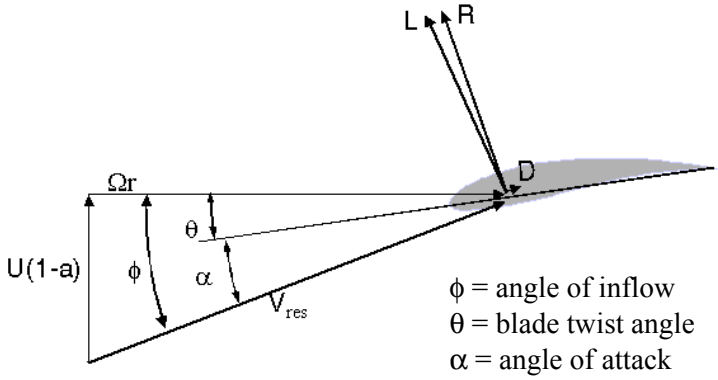

Figure 14: velocities, angles and forces on a blade element

The calculation procedure is iterative: start with an assumed induction factor, calculate the aerodynamic forces on the blade elements, sum the blade elements in the annulus,

derive a new induction factor in the annulus from the total force, and so on, until convergence is reached. Wilson and Lissaman (Ref. 7) made Glauerts theory applicable for modern computational approaches.

For the designer, the independent variables Ω, θ, U, the aerofoil characteristics L(α) and D(α), and the number of blades are available for design-optimization. Ω and U are linked by the tip speed ratio, defined by:

$$\lambda = \frac{\Omega R}{U} \qquad [17]$$

According to [11] the power coefficient C_p for a disc is a function of the induction a alone. From figure 14 it is clear that, for a given aerofoil, the induction depends on λ and θ, by which the power (coefficient) becomes:

$$C_p = C_p(\lambda, \theta) \qquad [18]$$
$$P = C_p(\lambda, \theta)\tfrac{1}{2}\rho U^3 \pi R^2$$

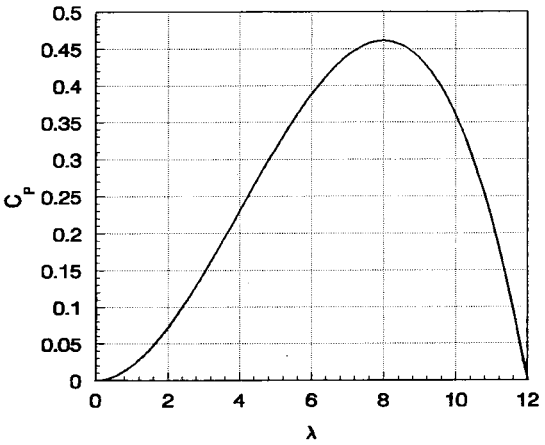

Figure 15: typical Cp(λ) curve for current wind turbines

Figure 15 shows an example of such a Cp(λ) curve for a given pitch angle. The maximum is below the theoretical maximum of 0.59, due to several losses. The drag of the aerofoil is a major contributor to these losses, but also losses due to the finite number of blades (the non-uniformity in azimuthal direction), and the rotation of the wake.

3.2 Aerofoil characteristics

One of the most important design choices concerns the aerofoil characteristics: the relation between lift & drag and the angle of attack. Figure 14 shows the vector diagram of a blade element, in which this angle of attack is defined. Aerofoil characteristics are measured in wind tunnels, under two-dimensional conditions (no flow in spanwise direction). Lift and drag are made dimensionless according to:

$$C_l = \frac{l}{\frac{1}{2}\rho U^2 c} \qquad C_d = \frac{d}{\frac{1}{2}\rho U^2 c} \qquad [19]$$

where c is the chord length. Figure 16 shows 2-D data from a typical wind turbine aerofoil. There is linear relation between C_l and α between (approximately) –10 and +10 degrees, where at the same time the drag coefficient C_d is minimal. This is the flow region in which the streamlines follow the aerofoil contour: attached flow. Above a certain limit (in the example of figure 16 $\alpha = 12^o$), the fluid elements cannot flow the contour any more, by which separated flow with high turbulence results. When the region of separated flow extends to the trailing edge of the aerofoil, this flow is called stalled flow. Some loss of lift is typical for stalled flow, and always a steep increase of drag.

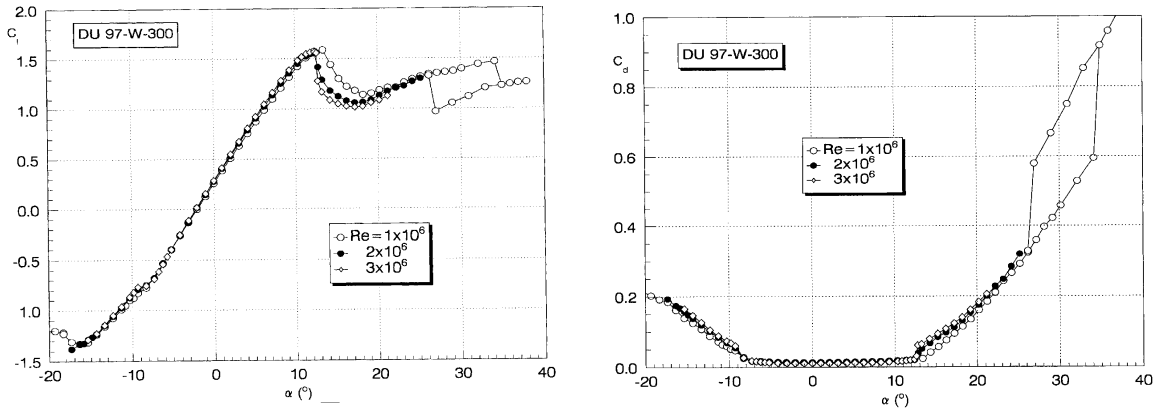

Figure 16: lift and drag characteristics of a wind turbine aerofoil.

The stall behavior is of utmost importance for wind turbines, for several reasons. Figure 17 shows the vector diagram of figure 14, but with an increased wind speed U. The angle of attack is increased, leading to an increased drag. The contribution to the torque of the rotor is again Lsinφ-Dcosφ, but by the increase of D, the torque and by that the rotor power, remains limited. This 'natural' load-limiting effect depends on the balance between Lsinφ and Dcosφ. Due to the inherent unsteady character of stalled flow, both terms fluctuate, leading to fluctuations in the power output.

Figure 17: blade element vectors in stalled conditions

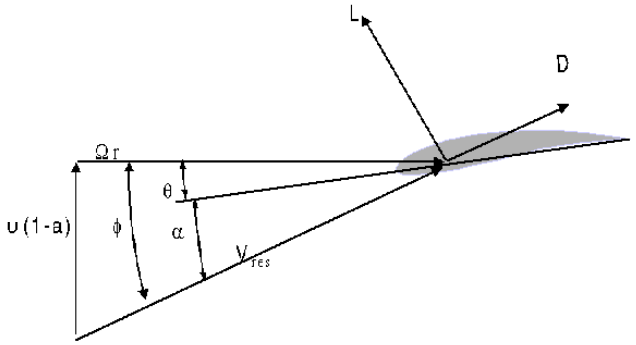

3.3. Unsteady aerodynamic characteristics and damping

The vector diagrams of figure 14 and 17 are simplifications of the real flow diagrams. The wind speed and direction vary continuously, the rotor speed is not very constant and the rotor blade moves under the aerodynamical and inertia forces. Rotor blades are flexible constructions, and are easily excited by aerodynamic loads. The interaction between dynamics and aerodynamics is called aeroelasticity, and is not discussed here. In this paragraph only the phenomenon 'aerodynamic damping' is introduced. This damping is of great importance for the rotor itself, but also for the dynamic behavior of the entire offshore wind energy converter.

Figure 18 shows schematically a blade with a flap angle β (flap is the out-of-rotor-plane direction). In static conditions the integrated aerodynamic and centrifugal loads balance the internal bending moments in the blade. Under dynamic conditions, due to varying V and/or varying β, the blade inertia comes into play. Suppose that the blade can freely hinge at the blade root r=0, then the equation of motion is:

$$I\ddot{\beta} + \Omega^2 I\beta = M_{aero}(t) \qquad [20]$$

with $$I = \int_0^R r^2 dm \qquad [21]$$

being the inertia of the blade with respect to the blade flapping axis. The aerodynamic moment contains a term proportional to the flap speed $\dot{\beta}$. This is clear from figure 19, which is equivalent to figure 14, except for the occurrence of a component of the relative wind speed due to the flapping motion: $V_{flap} = r\dot{\beta}$. Suppose the blade moves in downwind direction due to a gust, then the relative wind speed $r\dot{\beta}$ is added to the real wind speed. As a consequence, the angle of attack decreases, leading to a change in lift and drag, and consequently, in the aerodynamic flapping moment. This speed-related term is called the damping:

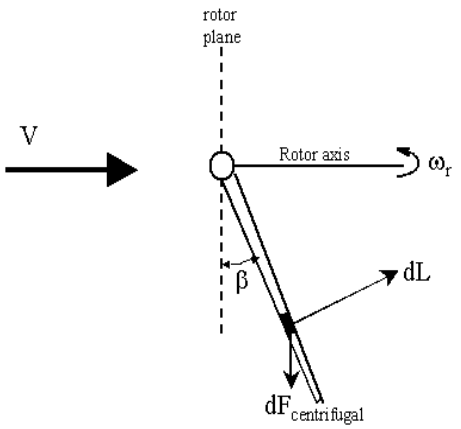

Figure 18: blade dynamics:due to the flapping motion $\dot{\beta}$, a relative wind speed $r\dot{\beta}$ is added to V

$$I\ddot{\beta} + (damping)\dot{\beta} + \Omega^2 I\beta = M_{aero}(t) \qquad [22]$$

Damping is positive when it works against the excitation. For attached flow this is the case. Consider figure 16 and suppose the lift coefficient is in the linear part of the curve (the part with attached flow). An increase in wind speed initially increases the flap angle β, which gives, in the coordinate system attached to the aerofoil, the velocity component $r\dot{\beta}$ as shown in figure 19. This component decreases the angle of attack α, consequently also the lift, so the flap motion is decelerated. For stalled flows, above α = 12°, the slope of the curve is negative. A decrease of α increases the lift, and accelerates the flapping motion. This is one of the main disadvantages of stalled flow: lack of, or even negative, damping.

In reality the interaction between blade dynamics and changes in wind speed is much more complicated. Stalled flow is intrinsically an unsteady process, and very sensitive to changes in angle of attack and to details of the geometry of the aerofoil. The prediction of unsteady aerofoil characteristics in stalled flow is one of the most difficult problems in rotor aerodynamics.

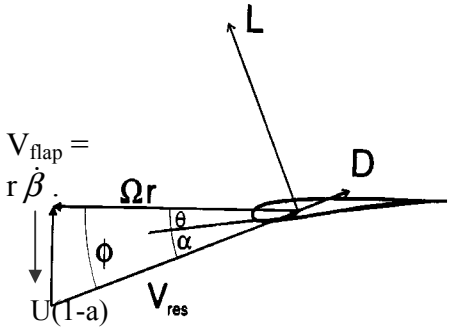

Figure 19: the effect of flapping motion on the angle of attack.

The above reasoning also holds for dynamic movements of the entire rotor instead of the flapping movement of one blade. Movements of the rotor in fore-aft direction yields similar vector diagrams as in figure 19, with $r\dot{\beta}$ replaced by the rotor fore-aft velocity , due to excitation of the support structure. A rotor with attached flow acts as a damping device for dynamic movements of the support structure. This is very important, not only for stability reasons, but in particular for minimizing the fatigue loads in the support structure, due to the hydrodynamic forces.

4. P-V curve and Power Control

4.1 The limitation of excess power in high wind speeds

According to [15], the power increases with the cube of the wind speed when the power coefficient is constant. This is possible by keeping the turbine running at constant tip speed ratio λ (the rotational speed is proportional to the wind speed). Many turbines operate at constant speed, by which $C_p \leq C_{p,max}$. Figure 20 shows the typical P-V curves.

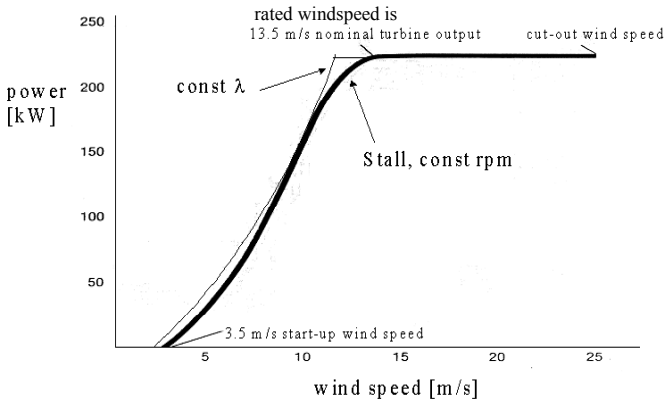

Figure 20: Typical P-V curves for constant Ω and constant λ turbines.

Both concepts, constant λ or constant Ω, require a mechanism for power limitation for high wind speeds. The wind speed at which the rated generator power is achieved, is called the rated wind speed. Power control above V_{rated} is one of the most important design choices, and determines the concept of the turbine. The three options are:

- Constant Ω turbines with stall control
- Constant Ω turbines with assisted stall control: the stall level can be adjusted by pitch changes
- Constant λ (so variable Ω) with pitch-to-feather control

In theory other combinations are also possible: constant λ with stall, or constant Ω with pitch-to-feather control. For various reasons these concepts are not successful, and will not be discussed here. The phenomenon of stall is explained in section 3.2. Figure 21 illustrates the effect of stall and pitch-to-feather.

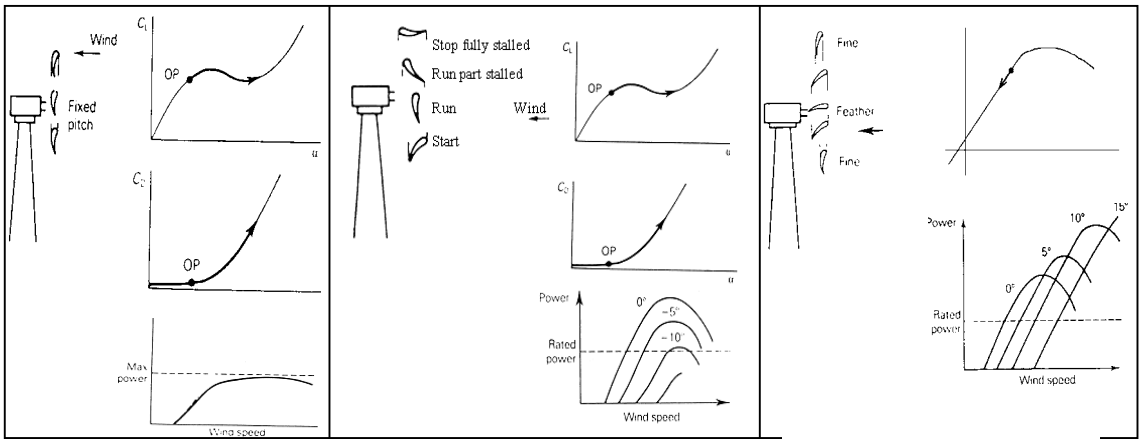

a: stall *b: assisted stall* *c: pitch to feather.*

Figure 21: several possibilities to limit the power in high wind speeds.

Constant Ω turbines with stall control (figure 21a):
Since the rotational speed and the pitch angle θ is fixed, an increase of wind speed increases the angle of attack α (see figures 14 and 17), by which the operating point (OP) in the lift and drag graphs shifts to the right: the lift remains approximately at the

same level, the drag increases sharply, by which the power is limited. As explained in section 3, the power level depends on the balance between the lift- and drag-component contributing to the torque of the rotor. Both components fluctuate continuously, by which the resultant power also fluctuates. Furthermore the associated blade bending moments are high. The simplicity of the system explains why this concept has been used with great success in almost all Danish turbines.

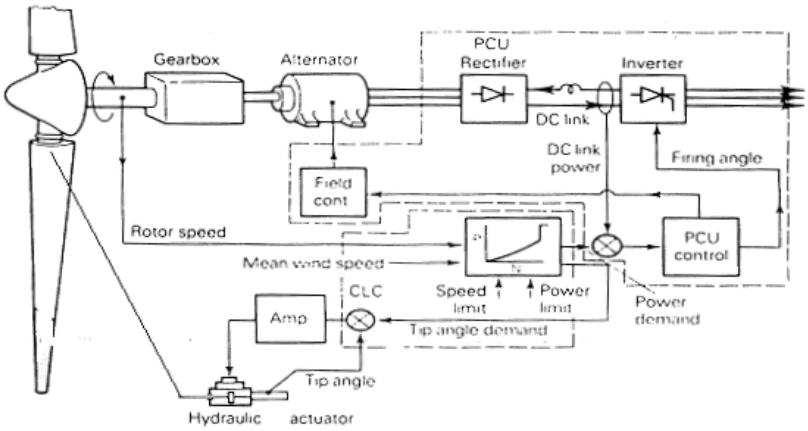

Figure 22: Schematic of a variable speed control system.

Constant speed with assisted stall (figure 21b):
The physical mechanism is identical, but the level of the stall can be tuned by changing the pitch angle θ. For increasing wind speed the pitch angle is adjusted in the direction of stall. This is not a continuous process: θ is changed as a function of the average wind speed, based on some time interval which is at least 10 minutes. The resultant power curve is composed out of (parts of) the power curves for several pitch angles.

Constant λ (so variable Ω) with pitch-to-feather control (figure 21c):
Pitch control in the direction of zero-lift (feather) diminishes the lift for increasing wind speed: the operating point at the lift curve shifts to the left. The drag remains low, and is not plotted in the figure. Again the power curve is a cross section through several power curves for constant pitch angle.

4.2 Power and load control under rated wind speed

This is only possible for turbines with pitch control to feather. It is usually combined with variable speed. Variable speed alone is enough to keep the turbine working at optimum efficiency $C_{p\text{-}max}$ by adjusting the rotational speed to the wind speed. For load control the combination of variable speed and pitch control offers the best opportunities. Pitch control alone is not fast enough: the time scale of turbulence is often different from the pitch rate of the blades. Then the pitch change can be out-of-phase with the changes in wind speed, causing an amplification of the disturbance. Combined with variable speed, the rotor inertia takes care of the fast changes: the kinetic energy of a gust is stored temporarily in the acceleration of the rotor and drive train. During this acceleration, the pitch angle is adjusted, by which a new equilibrium between wind speed and rotational speed is set. By changing Ω and θ continuously, a very smooth power and load control is possible. The control of Ω is done through the power electronics required for the variable speed operation. Figure 22 shows a schematic lay-out of such a control system. The input parameters for the control are V, Ω, design P-V curve, DC power, the output parameters are θ, generator field strength, inverter fire angle. By fine-tuning of the power electronic parameters, also high

requirements on power quality can be met: reactive power, voltage and frequency variations, harmonic fluctuations can be adjusted to the requirements of the grid operator. A detailed description of the control possibilities is outside the scope of this chapter.

4.3 Safety systems

Each wind turbine is equipped with a safety system of two levels. The safety system is allowed to overrule the control system, not vice-versa. The safety has evoluated from two distinctly different systems (e.g. an aerodynamical brake and a mechanical brake) to a more integrated and sophisticated approach. Most MW turbines have adopted the following system:

- Control: collective pitch adjustment, either for assisted stall control or for pitch-to-feather control.
- First safety level: collective pitch change at a high angular velocity, either to stall or to zero lift.
- Second safety level: individual pitch change at a high angular velocity, either to stall or to zero lift.

This second level requires that each blade have an independent pitch control mechanism, with independent energy backup. In practice this implies a control computer, energy supply and pitch actuator for each blade. One of the (usually 3) blades is allowed to fail: the remaining blades should be able to bring the rotor in a safe position when necessary.

4.4 Concept comparison

In brief:

- Constant speed, stall control has the advantage of simplicity, and by that, relatively low turbine costs. The power control possibilities are limited (only possible by assisted stall) and the associated loads are high. This is the concept with which the Danish manufacturers established their world-wide dominancy on the market.
- Variable speed, pitch control offers good control possibilities, including peak shaving of rotor and drive train loads. The electric conversion system is much more complex, since the variable frequency of the generator has to be converted to the grid frequency. The power electronic components are expensive, although prices are coming down. Most manufacturers of MW turbines have switched to this concept, mainly because of the better control possibilities.

5. Energy production

Each calculation of the yearly energy production requires knowledge of the statistics of the wind speed, see section 2.3. Here it is assumed that the frequency distribution f(V) of the wind speed is known. When also the power curve of the turbine is known, the yearly energy production E is calculated according:

$$E = T \int_{V_{ci}}^{V_{co}} P_{el}(V) \cdot f(V) dV \qquad [23]$$

where T is the number of hours in a year, and V_{ci} , V_{co} are the cut-in and cut-out wind speed respectively.
The graphical representation of [23] is shown in figure 23. The parameters available for maximalisation of E(V) for a turbine with a given rated power are:

- The type of power curve, preferably constant λ, maximal C_p below rated wind speed,
- The values of V_{ci} and $V_{co,}$
- The value of V_{rated}.

Figure 23: Graphical presentation of the distribution of the energy production distribution

To illustrate the impact of these parameters, the following train of thought is set up. Suppose that it is possible to construct a turbine that has no upper limit on the generator power, and no cut-in or cut-out wind speed. Then all energy in the wind could be extracted, limited only by the efficiency of the rotor and the drive train. When the Weibull wind distribution parameter k is taken to be 2 (the value for most north-west European cost lines), it can be calculated that the energy yield is:

$$E = 1.92\ C_{p,\max}\eta_{drivetrain}\frac{1}{2}\rho\overline{V}^3\pi R^2 T \qquad [24]$$

This describes the maximal output in a Weibull k=2 wind climate. In reality, the factor e=1.92 is less, due to the choices of V_{ci} , $V_{co,}$and V_{rated}. In figure 14 this is shown graphically.
The upper curve shows the energy content in the wind: $f(V)V^3$. Due to the efficiency of the rotor (0.45) and of the drive train (assumed 0.93) the energy content extracted by the ideal, imaginary turbine is about 60% lower. The content of this curve is given by the factor e = 1.92. Now real values for cut-in, and cut-out and rated wind speed are

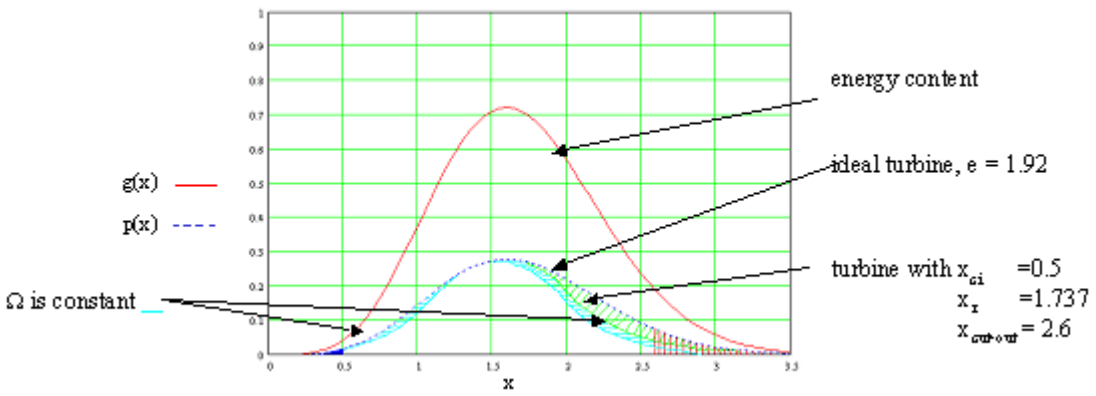

Figure 24: the distribution of the energy content in the flow, and the distribution of the extracted energy. Horizontal axis: $x = V/V_{average}$ Vertical axis: normalized energy content.

introduced. The choice of rated wind speed, above which the generator power is kept constant, introduces significant losses. The cut-in and cut-out wind speed are responsible for more, but less severe, losses. Finally, some additional losses are displayed (very exaggerated!) for a constant speed turbine that operates with $C_p \leq C_{p,max}$ below V_{rated} and a sub-optimal power control above V_{rated}.
For current variable speed turbines the value of e is about 1.35, instead of 1.92. Approximately $1/3^{rd}$ of the energy available in the wind cannot be extracted due to limitations on generator power and the necessity to limit the loads on the construction that are associated to the unlimited power extraction. The choices for V_{rated} and $V_{cut\text{-}out}$ have the highest impact on the energy production.

6. References

1. Burton, Sharpe, Jenkins, Bossanyi, *Wind Energy Handbook*, John Wiley and Sons, LTD, 2001
2. Wieringa, J. , Rijkoort, P.J., *Windklimaat van Nederland [In Dutch],* KNMI, 1983.
3. Troen, I., Petersen, E.L., *European Wind Atlas*, Risø National Laboratory, 1989.
4. A. Betz, *Das Maximum des theoretisch möglichen Ausnützung des Windes durch Windmotoren*, Zeitschrifft für das gesamte Turbinewesen, Volume 26, p.307, 1920.
5. F.W. Lanchester, *A contribution to the theory of propulsion and the screw propeller*, Transactions of the Institution of Naval Architects, Volume 57, p.98, 1915
6. H. Glauert. *Windmills and Fans.* In W.F. Durand (ed). Aerodynamic Theory Dover Publications Inc., New York 1963
7. R.E. Wilson and P.B.S. Lissaman. *Applied Aerodynamics of Wind Power Machines.* Oregon State University Report NSF/RA/N-74113, 1974.